IOSR Journal of Applied Physics (IOSR-JAP)
e-ISSN: 2278-4861.Volume 6, Issue 6 Ver. III (Nov.-Dec. 2014), PP 59-69
www.iosrjournals.org

Dielectric and magnetic investigations on novel P-2 type layered oxides

Soumava Palit
Tifr Centre for interdisciplinary studies(TCIS),Hyderabad-500075

Abstract: *This paper is about the investigation and analysis of dielectric and magnetic properties of the curious and promising P-2 layered oxides mainly for electrodes in rechargeable batteries.A solid state synthesis of the novel materials is taken up by taking NFMO as the guiding standard.Two more variants NMCO and NFCO are also synthesized.The structure is confirmed by xrd.The dielectric properties are studied by the cryostat apparatus and a high dielectric constant is observed.In the magnetic studies done by SQUID there is no long range magnetic ordering observed ,but an antiferromagnetic like transition is seen.*
Keywords: *Antiferromagnetic, Characterization, Dielectric, Layered material, NFMO, NMCO, NFCO, Solid state reaction.*

I. Introduction

Layered oxides are the subject of intense studies either for their properties as electrode materials for high-energy batteries or for their original physical properties due to the strong electronic correlations resulting from their unique structure.

1. Types of layered compounds:

The layered Na_xMO_2 materials can be categorized into two major groups which are P2 and O3 type. The first letter "P" or "O" refers to the nature of the site occupied by alkali ion (prismatic or octahedral), and "2" or "3" refers to the number of transition metal layers in the repeat unit perpendicular to the layering. The larger Na-ion is stable in the more spacious prismatic site. The material chosen in this work is $Na_{2/3}Fe_{1/2}Mn_{1/2}O_2$ which was reported in the journal nature and shows a better electrode performance.

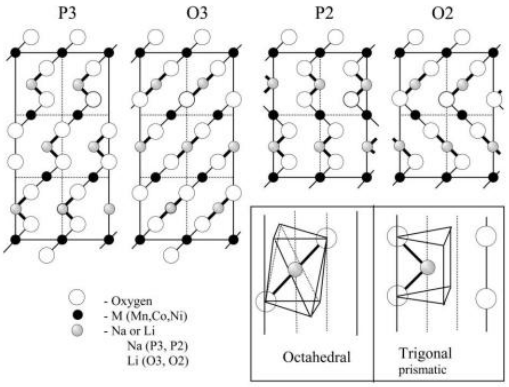

Fig 1.1 Different types of layered structures: P3, O3, P2, O2 &Octrahedral&Prizmatic sites are shown.[Ref.JMC 2003,13]

II. Structure:

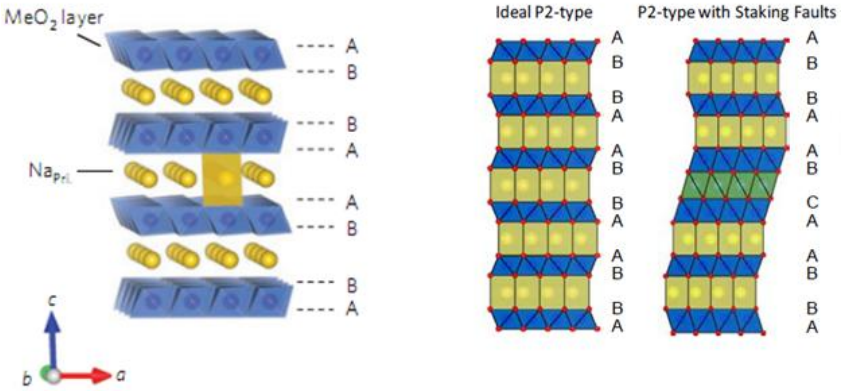

Fig 1.2 $Na_{2/3}[Fe_{1/2}Mn_{1/2}]O_2$ structure[Ref: Komaba et.al, Nature Materials 11 (2012) 512]

The $Na_{2/3}[Fe_{1/2}Mn_{1/2}]O_2$ structure consists of a hexagonal lattice with space group P63/mmc, which is structural with P2-type Na_xCoO_2. The a, b, c parameters a=2.9335(3) andc=11.224(1)Å) can be given. Sodium ionsare accommodated in prismatic sites. Symbols A and B in the schematic diagram depicts the two different oxygen layers described by the AB notation. A longer interlayer distance is observed for the P2 phase because of the repulsive electrostatic interaction of the AA-type oxygen stacking to form prismatic sites. If one had tried to increase the Fe percentage instead of Mn then, Fe4+ cannot be stabilized in the oxide-ion frame under ambient conditions. Hence the compound is regarded as a manganese (substituted) version of $NaFeO_2$.

2.1 Existence of a stacking fault:

It is interesting to note that the peak profile of $Na_{2/3}[Fe_{1/2}Mn_{1/2}]O_2$ cannot be fitted by a conventional profile function, such as a pseudo-Voigt function. From the XRD it is observed that the peak profile of (10l) lines is distinctly broad, especially at the bottom of each peak, whereas a typical peak profile is observed for (hk0) and (00l) lines, which are normal and parallel to the metal planes, respectively. Therefore a through plane stacking fault is observed in this p-2 type layered compound. The model for the stacking fault is shown in the figure.1.2.

III. Experimental:

3.1Dielectric mechanism

3.1.1 Capacitance, Dielectric Constant and polarization

Capacitance (C) is a measure of how much electric charge can be stored in a capacitor. The relationship between capacitance C and dielectric constant ε_r (k) in parallel plate geometry is given by the following equation:

$C = \varepsilon_o \varepsilon_r A/d$

Where $\dot{\varepsilon}_o$ is the dielectric constant of the free space (8.854 * 10-12 F/m), A is the area of the electrical conductor, d is the thickness of the dielectric layer, and $\dot{\varepsilon}_r$ is the dielectric constant of the dielectric layer. It is evident that the larger the dielectric constant, the larger the capacitance which can be realized in a given space.

The ability of the dielectric materials to store energy is attributed to the polarization, i.e. electric-field induced separation and alignment of the electric charges, which can result in an increase in capacitance. There are several molecular mechanisms associated with this polarization, including electronic, ionic, molecular (dipole), and interfacial (space-charge) polarisation. In general application of a field to each of these mechanisms in a normal state will cause displacement of charge which results in a polarization in the direction of the field. This effect on each mechanism can be seen schematically in fig1.4. For a given material, the sum of the contributions from each mechanism determines the net polarization, P, of the dielectric material.

P = **P**electronic + **P**ionic + **P**molecular + **P**interfacial

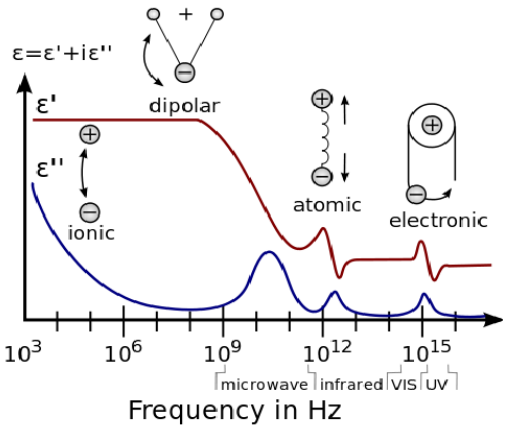

Fig1.3 Frequency dependence of polarization processes.

3.2 Dielectric Loss

The dielectric loss is a measure of energy loss in the dielectric during AC operation, which is a material property and does not depend on the geometry of capacitor.Usually the dielectric loss, expressed as the loss tangent (tan δ) or dissipation factor (D_f) can be defined as

$$\tan \delta = \frac{\varepsilon''}{\varepsilon'} + \frac{\sigma}{2\pi f \varepsilon'}$$

Whereε', ε", are the real and imaginary part of the dielectric permittivity and σ is the electrical conductivity of the materials, respectively, and f is the frequency.

In general, dielectric loss of the dielectric material is resulted from distortional, dipolar, interfacial, and conduction loss. The distortional loss is related with electronic and ionic polarization mechanisms. The interfacial loss originates from the excessive polarized interface induced by the fillers and specifically the movement or rotation of the atoms or molecules in an alternating electric field. The conduction loss is attributed to the dc electrical conductivity of the materials, representing the flow of actual charge through the dielectric materials.

3.3 Measurement and instrument condition

To perform the temperature variation of capacitance/dielectric measurement, a homemade capacitance probe that can fit in the commercial cryogen free superconducting magnet system (Model No. 5TL-VRTB30, Janis Research Company, USA) was used.However only LN2 was used as the measurements were taken only till 100Kthe probe was designed with an aluminium flange and hollow stainless steel (SS) rod. The Sample was mounted on a copper block; to prevent the electrical conductivity and to keep good thermal contact, a thin mica sheet was placed in between the sample and the copper block. All the measurements were performed on two point configuration a. Teflon coated SS coaxial cables were connected to the BNC connectors attached to the aluminium flange. The inner part of the coaxial wire is connected at the bottom of the probe to the sample holder. The two ends of the outer shielding wires were connected to the copper block at the bottom of the holder and aluminium flange at the top; this keeps the entire probe at the sample potential. For temperature and field dependent capacitance/dielectric measurements/impedance measurements, probe was inserted into the superconducting magnetsystem or LN2 depending on the temperature sought. Temperature was measured using the Lakeshore temperature controller (Model 332) that displays and controls the sample temperature. A calibrated Cernox sensor is used for temperature measurements. For capacitance/dielectric measurements, sample was made into parallel plate geometry where both sides of the sample were coated with highly conducting silver paste. In the parallel plate geometry here, C stands for capacitance and Tanδ indicates loss tangent. In the present study to maintain the parallel plate geometry (area >> thickness) the disc shaped samples are prepared with diameter of 13 mm and thickness of 1-1.5 mm. The capacitance measurements were performed either Agilent impedance analyzer (Model No.4294A, USA) or Hioki LCR bridge (Model No.3532-50, Japan) in the frequency range 40 Hz-1MHz under the ac field of 20 mV-1 V and dc field of 0 V-10 V.

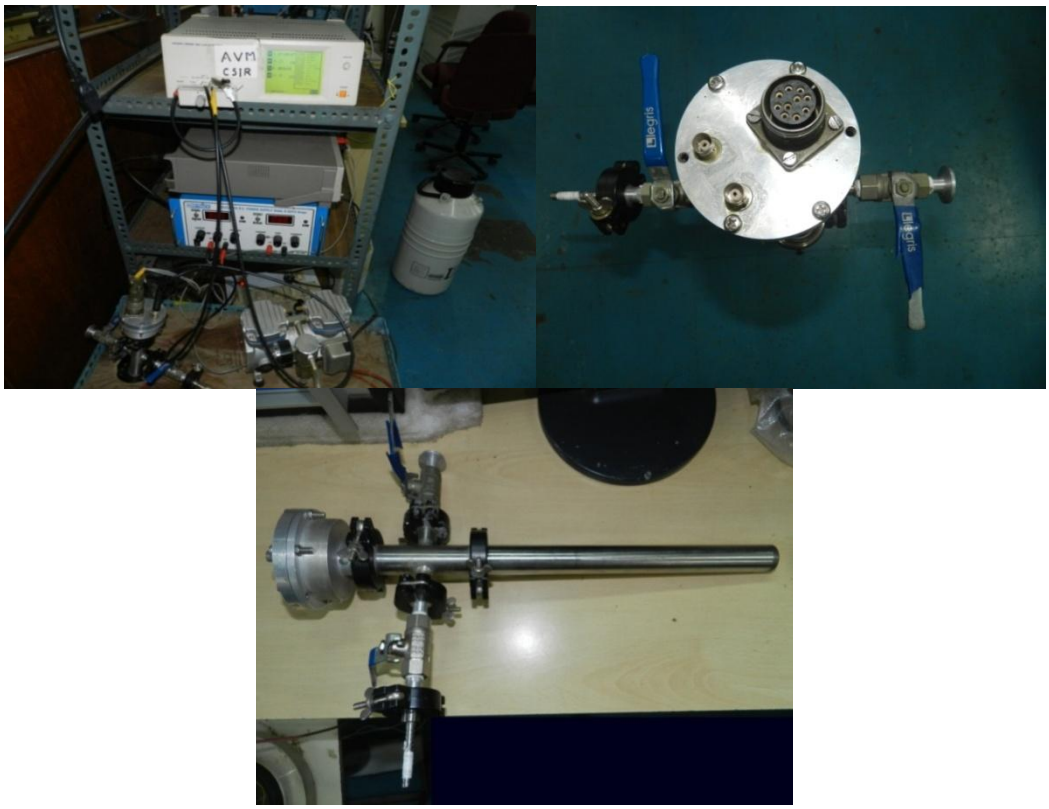

Fig 1.4:Dielectric and cryostat apparatus used.

SQUID: The superconducting quantum interference device (SQUID) magnetometer is based on the principle of the measurement of the flux change through a pick up coil. The signal is proportional to the magnetic moment of the sample.
The main components of a SQUID magnetometer are:

1. Superconducting magnet,
2. pick up coil (superconductingdetection coil) which is coupled inductively to the sample,
3. A SQUID connected to the detection coil and
4. A superconducting magnetic shield.

The detection coil is a single piece of superconducting wire arranged as a second-order gradiometer. This pick up coil system is positioned in the uniform magnetic field region of the solenoid superconducting magnet. High sensitivity is possible in a SQUID because this device responds to a fraction of the flux quantum. A measurement is done in this equipment by moving the sample through the pickup coil. The magnetic moment of the sample causes a change in the magnetic flux in these coils thereby inducing a current in them. This in turn changes the persistent current in the detection circuit, producing variation in the SQUID output voltage proportional to the magnetic moment of the sample. The SQUID is a parallel circuit of two Josephson junctions. A Josephson junction is a weak link between two superconductors that can support a super-current below a critical value. The special properties of the Josephson junction cause the impedance of the SQUID loop to be a periodic function of the magnetic flux threading the SQUID. In practice, the flux through the SQUID loop is held constant by a negative feedback using an additional coil. The SQUID functions as a flux to voltage converter.

Fig 1. 5Superconducting Quantum Interference Device (SQUID)

A Quantum Design MPMS SQUID VSM was used for the investigation of the ac and dc magnetic properties of all the studied samples. The combination of vibrating sample magnetometer with the sensitivity of a SQUID makes this system more versatile and unique; where the measurement can be performed at high speed (max 30K/min and 700 Oe/sec) with high sensitivity of 10^{-8} emu. Ac susceptibility measurements can be done from 0.1Hz to 1KHz with the sensitivity of 5 x $l0^{-8}$ emu at 0T. Measurements were carried out on powder samples, which were wrapped on the Teflon tape and was formed into a cylindrical shape (diameter of 2mm length of 6 mm) to minimize the demagnetization factors.

IV. Synthesis

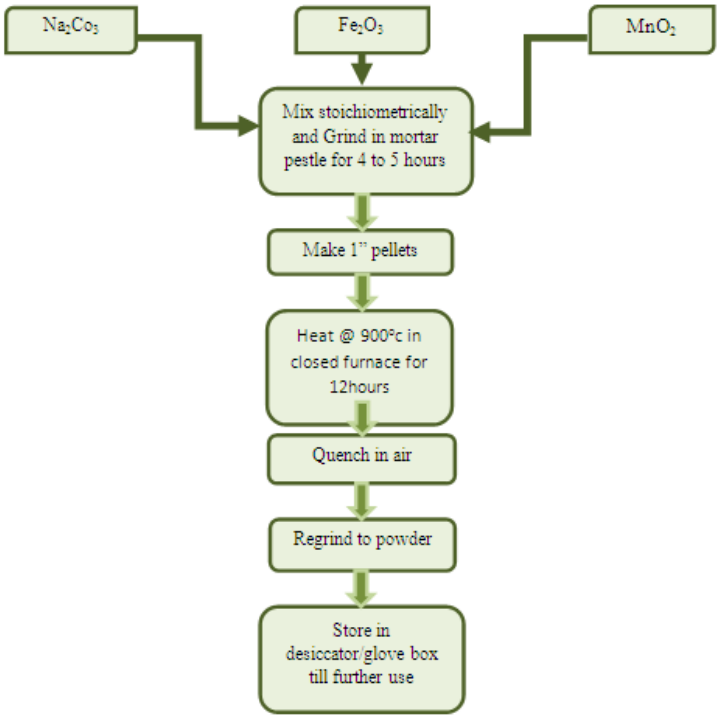

Fig 1.6 Flow chart for solid state preparation

4.1 Solid state reaction:

The mostly widely used method for the preparation of polycrystalline solids (i.e. powders) is the direct reaction, in the solid state, of a mixture of solid starting materials. Herein we use the same method at high temperatures. Solids do not usually react together at room temperature over normal timescale and it is necessary to heat them to much higher temperature often 1000 to 1500^{o}C, in order for reaction to occur at an appreciable rate. This shows both the thermodynamics and kinetic factors are important in solid state reaction; thermodynamics consideration show whether or not a particular can occur and kinetic factors determine the rate at which the reaction occurs. The following two points are noteworthy.

a. There is a considerable differences in structure between reactants and products and

b. That there is a large amount of structural reorganization that is involved in forming the product: bonds must be broken and reformed and atoms must migrate, perhaps over considerable distances (on an atomic scale). Only at very high temperature do such ions have sufficient thermal energy to enable them occasionally to jump out of their normal lattice sites and diffuse through the crystal.

Fine grained materials should be used to maximize surface areas and hence reaction rates. Hence the grinding of the powder is very important. Mixtures should be heated first at a temperature for a few hours so that decomposition occurs in a controlled manner. This is because during heating, sintering and grain growth of both reactant and product phases usually occur in addition to the main reaction, causing a reduction in the surface area of the mixture. The reaction rate may also be speeded up by pelletizing the samples prior to heating, thereby increasing the areas of contact between the grains.

The products of solid state reactions are usually in the form of a powder or a sintered, polycrystalline piece. The flow chart depicts the vital steps in the synthesis. The XRD serves to indicate whether the reaction is complete, therefore, by showing that the original reactants have disappeared and by showing that unwanted side-products or intermediates have not formed.

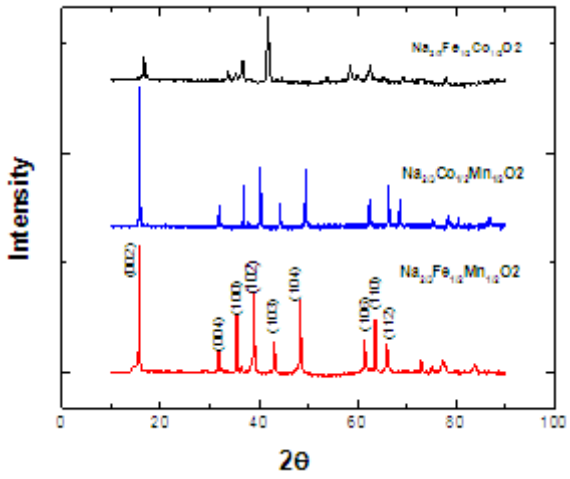

Fig 4.1 XRD data for nfmo,nmco and nfco

4.2 XRD

The XRD of NFMO obtained is in good agreement with the reported literature. In comparison NFCO shows multiphase due to the temperature being 900^{o}C for the solid state reaction. NFMO has a stacking fault and hence is a defect structure and thus cannot be fit by available functions (like pseudo VOIGT).

4.3 Dielectric studies:

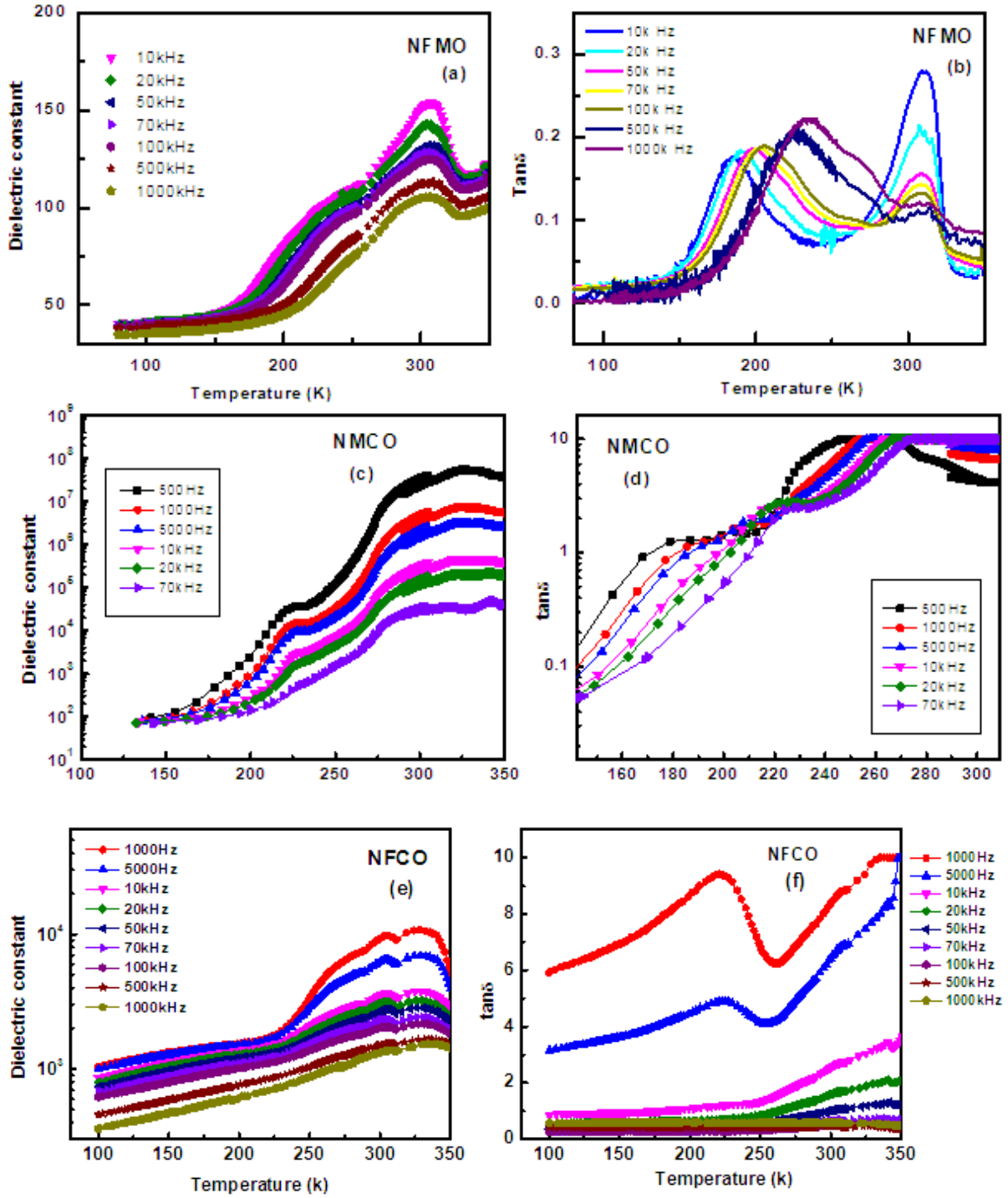
NFMO
(a)
10kHz
20kHz
50kHz
70kHz
100kHz
500kHz
1000kHz
Dielectric constant
Temperature (K)
NFMO
(b)
10k Hz
20k Hz
50k Hz
70k Hz
100k Hz
500k Hz
1000k Hz
Tanδ
Temperature (K)
NMCO
(c)
500 Hz
1000Hz
5000Hz
10kHz
20kHz
70kHz
Dielectric constant
NMCO
(d)
tanδ
NFCO
(e)
1000Hz
5000Hz
10kHz
20kHz
50kHz
70kHz
100kHz
500kHz
1000kHz
Dielectric constant
Temperature (k)
NFCO
(f)
tanδ
Temperature (k)

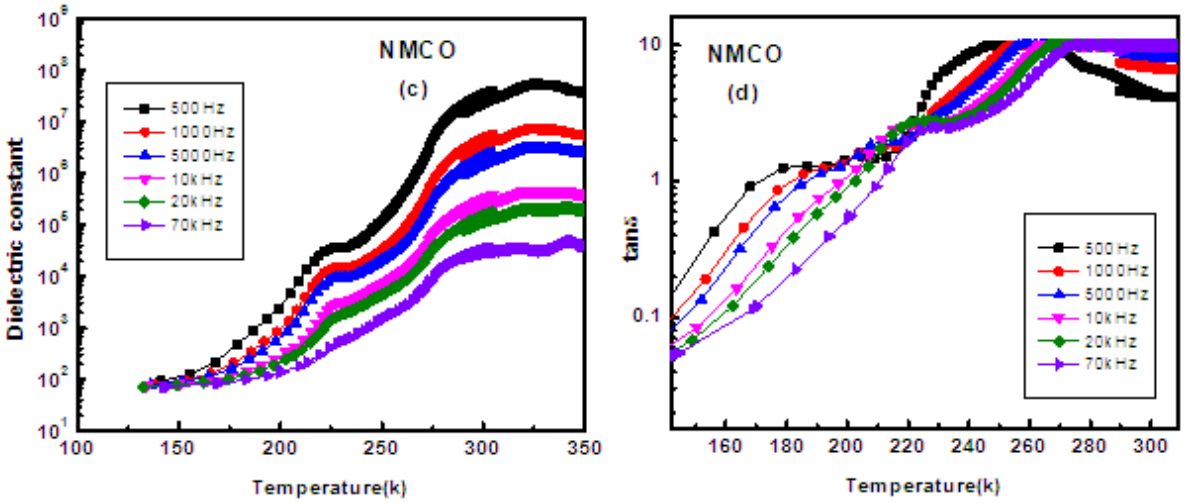

Fig4.2 Dielectric data for the samples

The dielectric constant is plotted as a function of temperature in the range 10-300k. In general relaxors contain permanent electrical dipoles. The peak position of dielectric constant coincides with the loss tangent peak. If there is a large separation between these two peaks the existence of permanent dipoles is ruled out.

4.3 Dielectric studies of NFMO:The dielectric constant is seen to increase on heating and reaches a peak at 300^{o}k. It attains a max value of 150 for the frequency of 10khz. The loss has 2 peaks one in the temperature range of 200 and other around 300.

The dielectric constants of NFCO and NMCO are high respectively 10^7 for NMCO and 5000 for NFMO. And when the Tan δ is high there is an enhancement in the sources of charge carrier in the system. The inter particle distances are less and the particles might be in contact which enhances the probability of charge transfer. Apart from this the amount of free charge carrier will also be higher. The electrical conductivity may also be enhanced. Any relaxation loss decreases the dielectric constant significantly and appears as a peak in the frequency. If there are other phases present as impurities the dielectric relaxation may be modified due to the other phase. This hints at colossal dielectric constants as observed in some transition metal oxides. The material with colossal dielectric constants are the focus of interest for the development of high dielectric material for modern electronics. The most prominent mechanism that can give rise to enhanced value of dielectric constant are ferro electricity, charge density wave formation, hopping charge transport, the metal insulator transition and various kinds of interface effects. In such materials charge carriers block at the interfaces exhibits a relaxationbehaviour similar to the Debye dipolar relaxation with respect to the temperature and frequency. High value of permittivity and its frequency dispersion has been assigned to the Maxwell Wagner interfacial polarization effects.

4.3 Squid : Magnetic Measurements

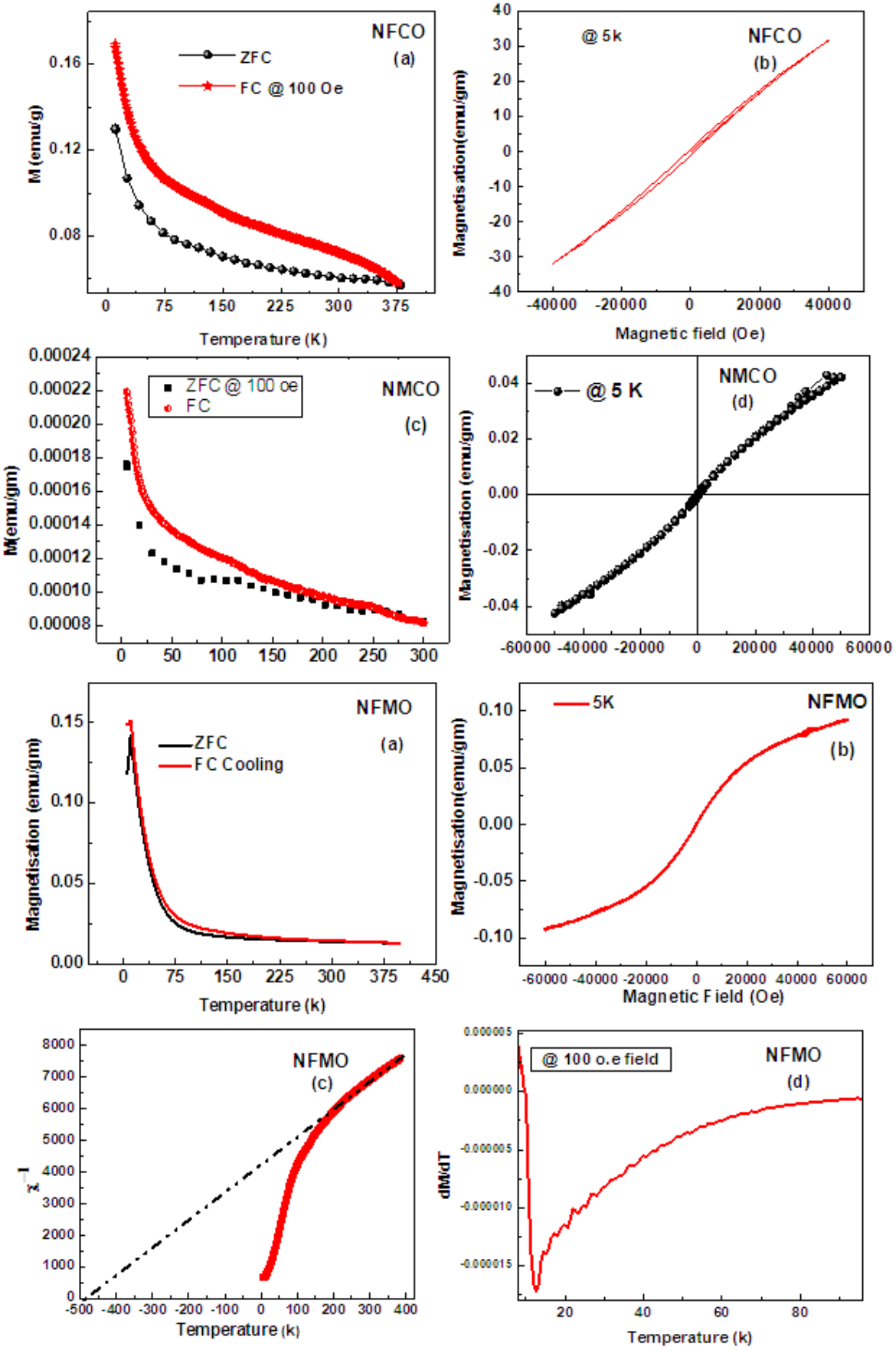

4.4 NFMO Magnetic behaviour:

The magnetic susceptibility, , is given within the mean-field approximation by the Curie-Weiss law, =C/ T−Tc,where C is a material-specific Curie constant, T is the absolute temperature, and the Weiss temperature Tc is the approximate temperature below which the system is ferromagnetic or antiferromagnetic, depending on the sign of Tc. In the Curie Weiss fit gives a Curie temperature of -487.494271 deg C. hence the sample is antiferromagnetic. A deviation from the Curie–Weiss law is observed, whose origin is unclear. Fig. 3bthe departure from the ideal fit occurs at 192.690192 deg C. There is an antiferromagnetic transition at the temperature of 12.708 as seen from the dM/dt curve.

The ZFC closely follows the fc curve. The m-h data shows neither hysteresis nor saturation tendencies. The Curie Weiss fit shows an intersection with the temperature axis, hence the sample is antiferromagnetic. The departure from the ideal fit occurs at 192.690192 K
There is an antiferromagnetic transition at the temperature of 12.708 K as seen from the dM/dt curve.

4.4.1 NFCO Magnetic behaviour:
The m-h curve shows a minimal hysteresis. The ZFC and FC do not overlap between 10k and 375k indicating interesting phenomena. There may be an anti ferromagnetic ordering at higher temperatures.

4.4.2 NMCO magnetic behaviour:
The gap between ZFC and FC is comparatively lower in NMCO as compared to NFCO. There is no hysteresis as seen from the m-h curve. Also there is no saturation behavior shows the magnetization versus field recorded at 5K, where no hysteresis is observed. Therefore no long-range magnetic order is achieved for P2-$Na_{2/3}Co_{2/3}Mn_{1/3}O_2$ in the 5–300 K temperature range.

4.5 Correlation of magnetic and dielectric data:
In Fig. 4, the temperature dependence of the dielectric constant ε, measured in the absence of external magnetic field, is presented. Using the plot of ε (T), one could clearly identify the transition temperatures which are not visible in small magnetization measurements.

V. NCMO SQUID

$Na_{2/3}Co_{2/3}Mn_{1/3}O_2$ phase. There is no difference in the temperature dependence of FC and ZFC magnetic susceptibility, indicating a paramagnetic behavior of the sample in the temperature range of 5–300 K. Fig. 3b shows the magnetization versus field recorded at 5 K, where no hysteresis is observed. Therefore no long-range magnetic order is achieved for P2-$Na_{2/3}Co_{2/3}Mn_{1/3}O_2$ in the 5–300K temperature range.

VI. Conclusion:

a) The solid state synthesis has the advantage the samples are easy to make.
b) The XRD results are obtained in good agreement with the reported literature but if the same temperature of heating is used for all the samples, certain samples may be more phases. This can be prevented by using a different temperature of synthesis or varying the proportion of the constituent elements.
c) The dielectric properties show one of the prepared samples(NMCO) to have very high dielectric constant. The loss tan δ is also correspondingly high.
d) The magnetic investigation using squid reveals the antiferro magnetic nature of NFMO. The magnetic behavior like M VS H and ZFC-FC is compared between the three samples.There is no detectable long range order in the NFCO and NMCO samples.
e) The explanation for the dielectric constants is complicated due to the interplay of a number of possible causative reasons.
f) Possible applications include intense studies either for their properties as electrode materials for high-energy rechargeable batteries particularly sodium ion rechargeable battery (the long proposedSuccessor to the lithium ion battery owing to safety, cost and abundance issues) or their original physical properties due to the strong electronic correlations resulting from their unique structure.

References

[1]. Ohzuku, T., Kitagawa, M. & Hirai, T. Electrochemistry of manganese-dioxidein lithium nonaqueous cell. 3. X-ray diffractional study on the reduction ofspinel-related manganese-dioxide. J. Electrochem. Soc. 137, 769775).(1990
[2]. Padhi, A. K., Nanjundaswamy, K. S. &Goodenough, J. B. Phospho-olivines aspositive-electrode materials for rechargeable lithium batteries. J. Electrochem.Soc. 144, 11881194 (1997).
[3]. Okada, S. et al. Layered transition metal oxides as cathodes forsodium secondary battery. ECS Meeting Abstr.602, 201 (2006).
[4]. Kim, D. et al. Enabling sodium batteries using lithium-substituted sodiumlayered transition metal oxide cathodes. Adv. Energy Mater.1, 333336 (2011).
[5]. Komaba, S., Takei, C., Nakayama, T., Ogata, A. &Yabuuchi, N. Electrochemicalintercalation activity of layered NaCrO2 vsLiCrO2 Electrochem.Commun.12,355358 (2010).
[6]. Komaba, S. et al. Electrochemical Na insertion and solid electrolyte interphasefor hard-carbon electrodes and application to Na-ion batteries. Adv. Funct.Mater.21, 38593867 (2011).
[7]. Newman, G. H. &Klemann, L. P. Ambient-temperature cycling of an NaTiS2cell. J. Electrochem. Soc. 127, 20972099 (1980).

[8]. Whittingham, M. S. Chemistry of intercalation compoundsmetalguestsinchalcogenide hosts. Prog.Solid State Chem. 12, 4199 (1978).
[9]. Abraham, K. M. Intercalation positive electrodes for rechargeable sodium cells.Solid State Ion. 7, 199212 (1982).
[10]. Delmas, C., Fouassier, C. &Hagenmuller, P. Structural classification andproperties of the layered oxides. Physica B+C 99, 8185 (1980).
[11]. Delmas, C., Braconnier, J. J., Fouassier, C. &Hagenmuller, P. Electrochemicalintercalation of sodium in NaxCoO2 bronzes. Solid State Ion. 34,165169 (1981).
[12]. Didier, C. et al. Electrochemical Na-deintercalation from NaVO2 .Electrochem.Solid-State Lett.14, A75A78 (2011).
[13]. Caballero, A. et al. Synthesis and characterization of high-temperaturehexagonal P2-Na0:6MnO2and its electrochemical behaviour as cathode insodium cells. J. Mater. Chem. 12, 11421147 (2002).
[14]. Berthelot, R., Carlier, D. &Delmas, C. Electrochemical investigation of theP2-NaxCoO2 phase diagram. Nature Mater.10, 7480 (2011).
[15]. Lu, Z. &Dahn, J. R. In situ X-ray diffraction study of P2-Na2=3TNi1=3Mn2=3UO2 .J. Electrochem. Soc. 148, A1225A1229 (2001).
[16]. Treacy, M. M. J., Newsam, J. M. & Deem, M. W. A general recursion methodfor calculating diffracted intensities from crystals containing planar faults.Proc. R. Soc. Lond. Ser.A 433, 499520 (1991).
[17]. Van der Ven, A., Aydinol, M. K., Ceder, G., Kresse, G. &Hafner, J.First-principles investigation ofphase stability in LixCoO2 .Phys. Rev. B 58,29752987 (1998).
[18]. Chen, Z. H., Lu, Z. H. &Dahn, J. R. Staging phase transitions in LixCoO2 .J. Electrochem. Soc. 149, A1604A1609 (2002).
[19]. Takeda, Y. et al. Sodium deintercalation from sodium iron-oxide. Mater.Res.Bull. 29, 659666 (1994).
[20]. Ado, K. et al. Preparation of LiFeO2 with -NaFeO2-type structureusing a mixed-alkaline hydrothermal method. J. Electrochem. Soc. 144,L177L180 (1997).
[21]. Hirayama, M., Tomita, H., Kubota, K. &Kanno, R. Structure and electrodereactions of layered rocksalt LiFeO2 nanoparticles for lithium battery cathode.J. Power Sources 196, 68096814 (2011).
[22]. Koyama, Y., Tanaka, I., Kim, Y. S., Nishitani, S. R. & Adachi, H. First principlesstudy on factors determining battery voltages of LiMO2 (M D TiNi).Jpn. J. Appl. Phys. 38, 48044808 (1999).
[23]. Senguttuvan, P., Rousse, G. l., Seznec, V., Tarascon, J-M. &Palacín, M. R.Na2 Ti3O7: Lowest voltage ever reported oxide insertion electrode for sodiumion batteries. Chem. Mater. 23, 41094111 (2011).
[24]. Komaba, S. et al. Fluorinated ethylene carbonate as electrolyte additive forrechargeable Na batteries. ACS Appl. Mater. Interf.3, 41654168 (2011).
[25]. Nishibori, E. et al. The large DebyeScherrer camera installed at SPring-8BL02B2 for charge density studies. Nucl.Instrum.Meth.467, 10451048 (2001).
[26]. Izumi, F. & Momma, K. Three-dimensional visualization in powder diffraction.Solid State Phenom.130, 1520 (2007).
[27]. Momma, K. & Izumi, F. VESTA: A three-dimensional visualizationsystem for electronic and structural analysis. J. Appl. Crystallogr. 41,653658 (2008).
[28]. Newville, M. IFEFFIT: Interactive XAFS analysis and FEFF fitting. J. Synchrot.Radiat.8, 322324 (2001).
[29]. Rehr, J. J. & Albers, R. C. Theoretical approaches to X-ray absorption finestructure. Rev. Mod. Phys. 72, 621654 (2000).